applied sciences

MDPI

Article

Development of New Functional Dense and Porous Materials from Opal Glass Cullet Through Mild Alkali Activation

Francesco Carollo [1,*], Emanuele De Rienzo [2], Antonio D'Angelo [3], Luisa Barbieri [2], Cristina Leonelli [2], Isabella Lancellotti [2], Michelina Catauro [3] and Enrico Bernardo [1,*]

[1] Department of Industrial Engineering, University of Padova, 35131 Padova, Italy
[2] Department of Engineering 'Enzo Ferrari', University of Modena and Reggio Emilia, 41125 Modena, Italy; emanuele.derienzo@univr.it (E.D.R.); luisa.barbieri@unimore.it (L.B.); cristina.leonelli@unimore.it (C.L.); isabella.lancellotti@unimore.it (I.L.)
[3] Department of Engineering, University of Campania 'Luigi Vanvitelli', 81031 Aversa, Italy; antonio.dangelo@unicampania.it (A.D.); michelina.catauro@unicampania.it (M.C.)
* Correspondence: francesco.carollo@unipd.it (F.C.); enrico.bernardo@unipd.it (E.B.)

Abstract

Opal glass, known for its mechanical strength, hygiene, and aesthetic appeal, contains fluorides that hinder recycling and often lead to landfilling. This study investigates the use of discarded opal glass for the production of sustainable alkali-activated materials (AAMs), contributing to waste valorization and reduced raw material consumption. By optimizing the activation process, dense products with high compressive strength, comparable to conventional concretes, were obtained using low-molarity alkaline solutions and low-temperature curing (60 °C). In addition, lightweight porous structures with porosity exceeding 80% were successfully produced through direct foaming and salt templating. The developed materials exhibited good chemical stability under aggressive conditions. Preliminary biological tests indicated antimicrobial activity and low toxicity, supporting their potential use in applications where hygiene and durability are important. The results highlight the versatility of mild alkali activation for transforming waste opal glass into dense and porous materials with tunable properties.

Keywords: opal glass; mild alkali activation; upcycling; salt-templating method; porous materials

1. Introduction

Opal glass, or milk glass, is a distinctive white and opaque material characterized by controlled light scattering due to crystalline or amorphous phases within its silicate matrix. These phases, often composed of fluorides and phosphates, are responsible for the opalescent appearance [1]. Opal glass balances opacity with mechanical and thermal properties, traditionally utilizing soda-lime silicate modified with fluorine, while recent advancements incorporate additives like titanium dioxide and zirconia to enhance performance [2]. Its unique properties allow for a wide range of applications, including lighting technology, laboratory equipment, and food-contact materials. Furthermore, its aesthetic appeal makes it popular in decorative arts and luxury packaging. Overall, opal glass serves as both a functional product and a cultural material, connecting industrial production with design heritage [1,2].

In recent years, recycling opal glass has become a crucial issue in the pursuit of sustainability and circular economy practices within the glass industry. However, its complex composition presents significant challenges for conventional recycling processes.

Academic Editor: Paulo Santos

Received: 22 April 2026
Revised: 26 May 2026
Accepted: 31 May 2026
Published: 3 June 2026

The presence of opacifiers and crystalline phases can interfere with the remelting process and potentially compromise the quality of recycled glass batches [1]. As a result, research has focused on developing strategies to reintegrate opal cullet into production cycles. These strategies include controlled dilution with transparent glass cullet, selective removal of problematic additives, and finding secondary applications for recycled opal glass [2]. Addressing these challenges is vital for reducing raw material consumption, minimizing waste, and lowering the carbon footprint of glass manufacturing.

Alkali-activated materials (AAMs) provide a sustainable solution for valorizing discarded glass, offering significant environmental and technical advantages. Due to its high amorphous silica content, finely ground waste glass can act as a reactive precursor in the alkali activation process. Here, alkaline activators like sodium hydroxide or sodium silicate induce dissolution and subsequent polycondensation reactions [3]. This process produces a hardened binder analogous to geopolymers, exhibiting favorable mechanical properties and durability [4]. Incorporating glass waste into AAMs helps reduce the accumulation of non-biodegradable glass in landfills and diminishes reliance on Portland cement, consequently lowering carbon emissions [5,6]. Additionally, AAMs derived from waste glass demonstrate high compressive strength, chemical resistance, and long-term stability, making them suitable for various construction applications [7,8]. Thus, utilizing waste glass in alkali activation aligns with circular economy goals and promotes the development of low-carbon building materials [9,10].

Besides dense blocks, porous materials and glass foams derived from alkali-activated glass waste have become promising alternatives to traditional lightweight insulating products, thanks to their low density, thermal resistance, and ability to valorize post-consumer residues [11,12]. In these systems, finely ground waste glass is partially dissolved in alkaline solutions, typically sodium hydroxide or sodium silicate, resulting in reactive gels that can bind and stabilize gas bubbles. These bubbles can be introduced either chemically, using agents like aluminum powder or hydrogen peroxide, or physically, through mechanical foaming [13,14]. The subsequent curing, and in some cases low-temperature sintering, produces a rigid porous network with tunable properties. Bulk densities can range from below 200 kg/m^3 to over 1000 kg/m^3, compressive strengths can vary from fractions of a megapascal to over 20 MPa, and thermal conductivities are often comparable to those of commercial insulating foams [15]. The microstructural features, such as pore size distribution, connectivity, and wall thickness, depend significantly on precursor particle size, activator concentration, and foaming agent dosage, making process optimization essential for balancing mechanical integrity and insulating performance [13,14].

This paper aims to explore the potential of waste opal glass in developing a new generation of alkali-activated materials, both dense and porous, that require no firing step, minimizing material and energy inputs. Specifically, we demonstrate the application of low-molarity sodium hydroxide and potassium hydroxide, as well as the use of coarse glass flakes to reduce milling needs. Sample hardening was conducted at low temperatures (not exceeding 60 °C) using microwave heating to shorten consolidation time and lower energy consumption [16]. Highly porous bodies, with total porosity exceeding 80%, were produced through direct foaming by incorporating foaming additives and surfactants into the activated glass, as well as via salt templating, where salt particles (inexpensive NaCl) were included and subsequently removed to create interconnected porosity. We carefully investigated the mechanical properties, chemical stability, antimicrobial activity, and cytotoxicity of the final products.

2. Materials and Methods

2.1. Production of Dense and Composite Samples

The starting materials consisted of residues from crushed opal glass, which were provided by Arc International (Arques, France). The glass composition was $72SiO_2$-$8Al_2O_3$-2CaO-2BaO-$12Na_2O$-$1.5K_2O$-$2.5F_2$ in wt.% [1]. The coarse opal glass was ground by dry ball milling using an agate jar (Changsha Deco Equipment Co., Hunan Yueyang, China) and sieved below 75 µm. Fine powders were mixed with an aqueous solution containing 2.5 M NaOH or KOH (reagent grade, Sigma-Aldrich, Gillingham, UK), using a liquid-to-solid ratio of 0.5, which was selected based on previous experience and process optimization [17]. Glass suspensions were mechanically stirred at 500 rpm for 3 h in polystyrene (PS) cylindrical containers to ensure both partial dissolution and homogeneous dispersion of glass particles. The resulting slurry was then poured into cubic silicone molds (10 mm^3 × 10 mm^3 × 10 mm^3) and left to dry for 24 h in a stove (Biomedica Elettronica, Padova, Italy) at 60 °C and subsequently cured with a domestic microwave (MJ3965BPS, LG, Samsung MS23F300EEK, Samsung Electronics Italia S.p.A, Milano, Italy) for 5 min at 450 W.

To produce composite materials, coarse LCD glass flakes (1 mm < Ø < 2 mm) and artistic soda-lime glass (SLG) were added to activated opal glass (described above) as an inert phase after mixing in a mass ratio of 1:1. The slurry was then poured into rectangular molds with dimensions 50 mm^3 × 40 mm^3 × 10 mm^3. LCD glass composition was SiO_2: ≥55 wt%, Al_2O_3: 15%, B_2O_3: 10%, CaO: 10%, SrO: 5%; BaO: 1% [18] whereas artistic SLG composition was SiO_2: 71.7 wt%, Al_2O_3: 0.7 wt%, Fe_2O_3: 0.1 wt%, CaO: 10.1 wt%, MgO: 3.3 wt%, Na_2O: 13.2 wt%, TiO_2: 0.1 wt%, K_2O: 0.1 wt%, SO_3: 0.2 wt% [19]. Glass suspensions were then treated as described above.

2.2. Production of Porous Samples

The porous samples were produced from opal glass powders activated only with sodium hydroxide, as it allowed better compressive strength results to be obtained. Two methods were used to produce the porous samples: direct foaming and salt templating. Direct foaming experiments involved mixing for 3 h followed by the addition of sodium perborate (SP) monohydrate ($NaBO_3 \cdot H_2O$, in an amount of 1 wt% relative to the mass of the glass powder). Foaming was optimized by adding an additional 1 wt% of sodium dodecyl sulfate (SDS, $CH_3(CH_2)_{11}$ OSO_3Na), a surfactant that acted as a stabilizer. The selected SP and SDS content was determined on the basis of previous studies concerning the production of porous materials by direct foaming of discarded glass and volcanic ash [20,21]. The obtained slurry was then dried in a stove at 60 °C for 24 h, followed by 5 min of microwave heating, and then characterized. The quantities of SP and SDS were gradually increased up to 2.5 wt% to obtain a total porosity of the consolidated material greater than 80%.

In the salt-templating method, coarse sodium chloride (NaCl) particles were ground with a mortar and sieved to obtain different grain size ranges from 0.5 to 2 mm. The quantities of salt particles with specific sizes were selected according to the Fuller curve, commonly used in concrete and granular packing design, in order to maximize packing density by combining coarse and fine particles in specific proportions and to promote the formation of an interconnected porous network after salt removal. Salt particles were added to the activated glass paste immediately after mixing, and the obtained suspensions were poured into silicone molds and then consolidated as described above. The amount of added salt was progressively increased from 70 wt% up to 120 wt% (relative to the mass of the glass powder). Samples containing 100 and 120 wt% salt, activated with 2.5 M NaOH, were extremely fragile. For this reason, in the last two formulations, the molarity of the alkaline

solution (NaOH) was increased to 5 M to improve the mechanical strength of the final porous material. After consolidation, the samples were immersed in distilled water and left in a stove at 60 °C for three days to remove salt from the matrix. The immersion water was changed every 24 h to prevent the deposition of dissolved salt from the solution onto the material. After the washing step, the specimens were dried in a stove at 60 °C for 24 h before being characterized. A summary of opal glass samples produced and characterized in this investigation is given in Table 1.

Table 1. Opal glass-derived samples.

Sample Name	Composition	Alkaline Activator	Production Process	Density (g/cm^3)	Number of Specimens
Dense NaOH	Opal glass (20 g)	NaOH 2.5 M (L/S: 0.5)	Stirring; stove + MW	1.47 ± 0.06	20
Dense KOH	Opal glass (20 g)	KOH 2.5 M (L/S: 0.5)	Stirring; stove + MW	1.46 ± 0.01	20
Composite LCD	Opal glass (20 g)–LCD glass (20 g)	NaOH 2.5 M (L/S: 0.5)	Stirring; stove + MW	1.76 ± 0.02	20
Composite SLG	Opal glass (20 g)–SL glass (20 g)	NaOH 2.5 M (L/S: 0.5)	Stirring; stove + MW	1.94 ± 0.01	20
Porous DF	Opal glass (20 g)	NaOH 2.5 M (L/S: 0.5)	Direct foaming (SP: 0.5 g; SDS: 0.5 g)	0.76 ± 0.05	20
Porous ST 70	Opal glass (20 g)	NaOH 2.5 M (L/S: 0.5)	Salt templating (NaCl: 14 g)	0.95 ± 0.06	20
Porous ST 80	Opal glass (20 g)	NaOH 2.5 M (L/S: 0.5)	Salt templating (NaCl: 16 g)	0.78 ± 0.02	20
Porous ST 90	Opal glass (20 g)	NaOH 5 M (L/S: 0.5)	Salt templating (NaCl: 18 g)	0.70 ± 0.03	20
Porous ST 100	Opal glass (20 g)	NaOH 5 M (L/S: 0.5)	Salt templating (NaCl: 20 g)	0.68 ± 0.01	20
Porous ST 120	Opal glass (20 g)	NaOH 5 M (L/S: 0.5)	Salt templating (NaCl: 24 g)	0.47 ± 0.01	20

2.3. Sample Characterization

The geometric density (ϱ_{geom}) of consolidated samples was evaluated by considering the mass-to-volume ratio of cubic samples (10 mm × 10 mm × 10 mm). The mass of the samples was measured with an analytical balance, and the volume was measured with a digital caliper. The apparent (ϱ_{app}) and the true density (ϱ_{true}) were measured by using an Ultrapyc 3000 helium pycnometer (Anton Paar S.r.l., Rivoli, Italy), considering bulk or

finely crushed samples, respectively. The three density values were used to compute the amounts of open and closed porosity, according to the following definitions:

$$\rho_{geom} = \frac{mass}{geometrical\ volume} = \frac{m}{GV}$$

$$\rho_{app} = \frac{mass}{apparent\ volume} = \frac{m}{GV - VOP}$$

$$\rho_{true} = \frac{mass}{true\ volume} = \frac{m}{GV - VOP - VCP}$$

where VOP and VCP are the volumes of open and closed pores, respectively. Fine powders obtained from crushed samples were obviously assumed to be pore-free. Combining the definitions, we obtained the following:

$$\frac{\rho_{geom}}{\rho_{app}} = \frac{\frac{m}{GV}}{\frac{m}{GV - VOP}} = \frac{GV - VOP}{GV} = 1 - f_{OP}$$

$$\frac{\rho_{geom}}{\rho_{true}} = \frac{\frac{m}{GV}}{\frac{m}{GV-VOP-VCP}} = \frac{GV - VOP - VCP}{GV} = 1 - f_{OP} - f_{CP}$$

The two equations (on density data) yielded the volume fractions of open and closed porosity, f_{OP} and f_{CP}. The determination of open and closed porosity was straightforward (open porosity = f_{OP} ·100%; open porosity = f_{CP} ·100%) [22].

Boiling tests were performed for all analyzed formulations by immersing the dry samples in a glass beaker with distilled water at 100 °C for one hour. The weight ratio of the mass of the sample to the amount of distilled water was 1:10.

The compressive strength of the cubic dried samples (both dense and porous) was measured according to the standard UNI EN 826 [23] using a Universal Testing Machine (Quasar 25, Galdabini S.p.a., Cardano al Campo, Italy), operating at a crosshead speed of 0.5 mm/min. The mechanical tests were performed immediately after the consolidation phase (combined stove and microwave treatment) and cooling (24 h at room temperature) of the samples. Six samples were tested for each formulation.

The mineralogical analysis of powdered samples was carried out using X-ray diffraction (XRD) (Bruker D8 Advance, Karlsruhe, Germany), with CuKα radiation (0.15418 nm), at 40 kV and 40 mA. The scan range was set from 2θ = 10° to 70°, with a step size of 0.05° and a 1 s counting time. Phase identification was performed using the Match!R program package (Crystal Impact GbR, version 1.11f, Bonn, Germany), with reference to data from the Powder Diffraction File (PDF)-2 database (International Centre for Diffraction Data, Newtown Square, PA, USA).

Scanning electron microscopy (SEM; JEOL JSM 7600 F, Tokyo, Japan, with 1.2 kV acceleration voltage) investigation, along with EDS analysis, was performed to examine the composition, morphology, and microstructure of dense and porous samples.

2.4. Leaching Tests

Leachate analysis was performed on the activated glass formulations to assess the degree of heavy metal stabilization within the matrices by quantifying their release after prolonged immersion in water. The leaching tests were conducted in accordance with the EN 12457 European standard for waste characterization [24]. Specifically, 5 g of each material was ground and sieved to a particle size below 2 mm, placed in Teflon containers, and submerged in distilled water at a solid-to-liquid mass ratio of 1:10. The suspensions were magnetically stirred for 24 h to ensure maximum exposure of the ground solids to the aqueous medium. After this period, the leachates were separated from the solid residues,

acidified to pH 2 using a nitric acid solution, and subsequently analyzed by inductively coupled plasma mass spectrometry (ICP-MS). Measurements were carried out with an iCAP TQ ICP-MS spectrometer (Thermo Fisher Scientific Inc., Waltham, MA, USA) with detection limits ranging from 10^{-3} to 10^{-1} µg/L. The leaching analysis consisted of three replicates for every formulation. For each sample, dilution factors were applied to the measured values in order to calculate the original ion concentrations in the leachates.

2.5. Cytotoxicity and Microbial Assays

Preliminary biological assays were performed only on dense and porous samples obtained by the salt-templating method. The cytotoxicity test was performed on human primary keratinocytes, HaCaT cells (as a eukaryotic epidermal cell model). The test was performed by assaying 1 and 2 mg of samples dispersed in cell media after cell growth and measuring cell viability inhibition (CVI, %) after 24 h of exposure. To this aim, HaCaT cell line was cultured at 37 °C in a humidified atmosphere with 5% CO_2, using Dulbecco's Modified Eagle's Medium (DMEM, Sigma-Aldrich, Milan, Italy) supplemented with 10% fetal bovine serum, 50 U/mL penicillin, and 100 µg/mL streptomycin [25]. Cells were seeded in 96-well plates at a density of 1.5×10^4 cells/well, and subsequently, cell viability was determined using the MTT assay, which quantifies the suppression of mitochondrial redox activity (CVI%) [26]. Negative values refer to an increase in HaCaT cell viability, whereas positive values mean a decrease in HaCaT cell viability and, thus, increased cytotoxic effects. Each condition was tested in triplicate, and data were reported as mean ± standard deviation (SD).

The antimicrobial activity of the samples was evaluated using a slightly modified Kirby–Bauer method, in which samples were placed directly onto Petri plates without using a filter [27]. To do this, all samples were finely ground and compressed into 200 mg discs, which were sterilized under UV light for 1 h and then placed in direct contact with a microbial suspension containing 10^5 CFU/mL. Two representative strains were tested: *Escherichia coli* ATCC 25922 (Gram-negative) and *Enterococcus faecalis* ATCC 29212 (Gram-positive). The bacteria were plated on their respective agar-based solid media and incubated both in the presence and absence (control) of the sample discs. Following microbial growth, the inhibition zones were measured, with four measurements performed for each Petri dish. Results were expressed as mean ± SD.

2.6. Statistical Analysis

For the statistical analysis, data obtained from the porosity and mechanical tests were analyzed and processed using MATLAB software (version R2025a). The porosity and compressive strength results of the samples fabricated via the salt-templating method were compared using a two-sample *t*-test with a significance level of 5% ($p < 0.05$).

3. Results and Discussion

3.1. Dense Products

The hardening of activated opal glass suspensions led to samples with a remarkable strength-to-density ratio, especially upon reaction with NaOH. Consolidated samples composed solely of opal glass, in fact, exhibited a density of 1.47 ± 0.06 g/cm^3 (corresponding to a porosity of ~40%) and a compressive strength of 30.3 ± 2.9 MPa. Samples activated with KOH displayed a comparable density (1.46 ± 0.01 g/cm^3), but significantly lower ($p < 0.01$) mechanical strength (22.2 ± 4.4 MPa).

The evolution of the samples was first studied by a combination of X-ray diffraction and SEM microscopy analysis. No transformation was observed for the fluoride crystals (NaF, PDF#89-2956; CaF_2, PDF#88-2301; BaF_2, PDF#85-1342) originally immersed in opal

glass (Figure 1a, for NaOH activation, and Figure 1c, for KOH activation). In contrast, some extra phases, both crystalline and amorphous, could be found. Hydrated alkali carbonates, from the interaction of activating solution with atmospheric CO_2 ($Na_2CO_3 \cdot H_2O$, PDF#70-2148, see Figure 1a,b, and $KH(CO_3)$, PDF#89-2369, see Figure 1c,d) emerged as new crystal phases after activation and disappeared after immersion in boiling water. The solubility of hydrated alkali carbonates is not surprising; the most remarkable finding concerns the slight modification of the background signal, attributable to the amorphous phase, which persisted after boiling (see Figure 1b,d: the patterns of the materials after boiling lost the peaks corresponding to carbonates, but they do not overlap with the pattern of the starting material). In our opinion, this could be due to the presence of an extra amorphous aluminosilicate gel phase resembling that formed in geopolymers [28] (with stability provided by a fully interconnected three-dimensional network of SiO_4 and AlO_4 units, the latter balanced by alkali ions).

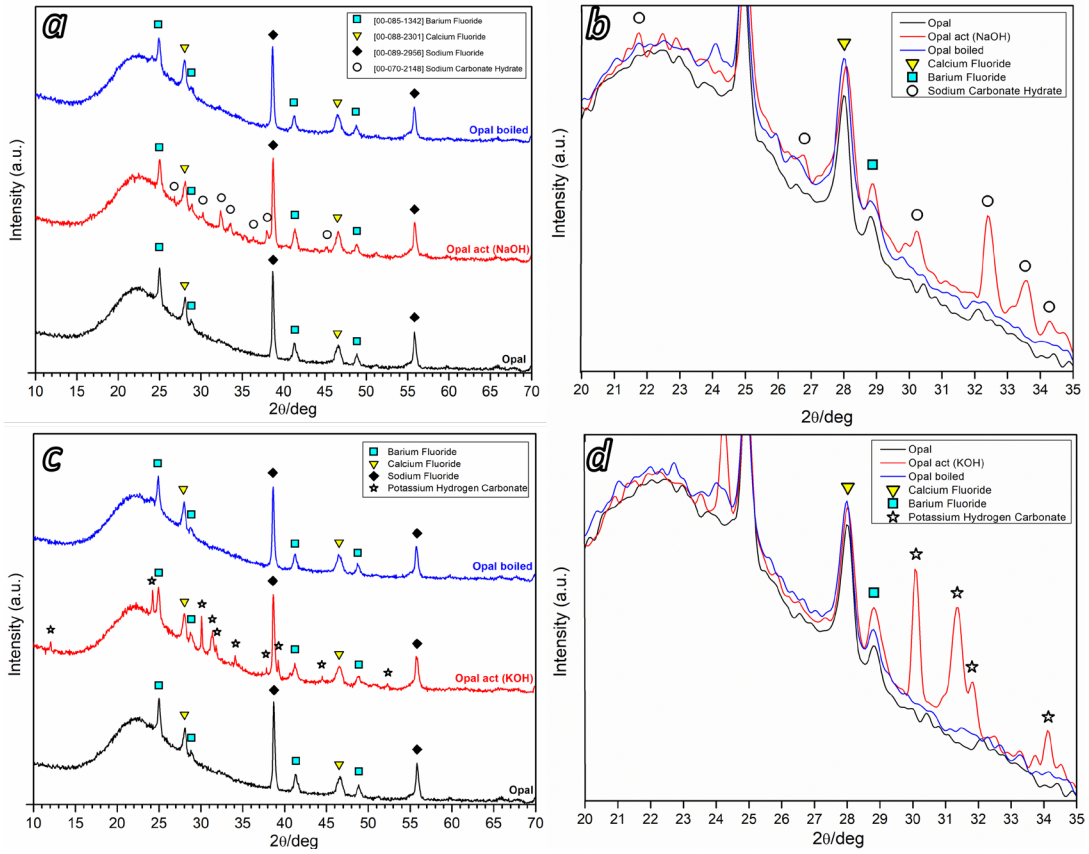

Figure 1. X-ray diffraction analysis of opal glass in the as-received state, after activation with 2.5 M NaOH (**a**) and 2.5 M KOH (**c**), and after boiling, with magnified overlapping patterns (**b**,**d**).

In other words, the behavior of opal glass, attacked by relatively diluted alkaline solution, can be considered as a sort of 'hybrid' between activated glasses and geopolymers. It has already been shown that during consolidation, glass particles create a structural 'skeleton' through condensation reactions involving surface Si–OH, Al–OH, and B–OH groups. These groups become available when OH^- ions cleave Si–O–Si, Si–O–Al, and Si–O–B bonds. A Si–OH group on the surface of one particle can react with a Si–OH group on another, forming a Si–O–Si bridge that links adjacent particles [29]. The products of glass dissolution may undergo condensation as well, but the resulting gel is as soluble in boiling water as alkali carbonates. Due to its particular chemical composition, opal glass evidently led to a more interconnected gel, particularly with NaOH, justifying the observed strength.

The magnified XRD spectra of the activated samples (Figure 1b,d) show that NaOH-activated glass promotes the formation of a greater amount of stable secondary phases than KOH activation. This difference in the reaction products suggests that sodium hydroxide enhances the dissolution and subsequent reorganization of the glassy matrix more effectively, leading to the development of a more stable and compact microstructure.

In contrast, the KOH-activated system appears to generate a lower quantity of these stable secondary phases, indicating a less extensive reorganization during the activation process. This distinct chemical and mineralogical behavior is consistent with the mechanical test results, where the NaOH-activated samples exhibit higher mechanical strength and improved resistance. In any case, independently of the hydroxide activator, hardened samples did not undergo disintegration after immersion in boiling water, suggesting the formation of strong interparticle bonds.

EDS analysis of the consolidated samples confirmed the presence of fluorides immersed in the amorphous matrix (Figure 2a, referred to as opal glass activated with NaOH). Alkali carbonates were easily detected in the activated samples (Figure 2b), whereas no trace could be found after the boiling test (Figure 2c).

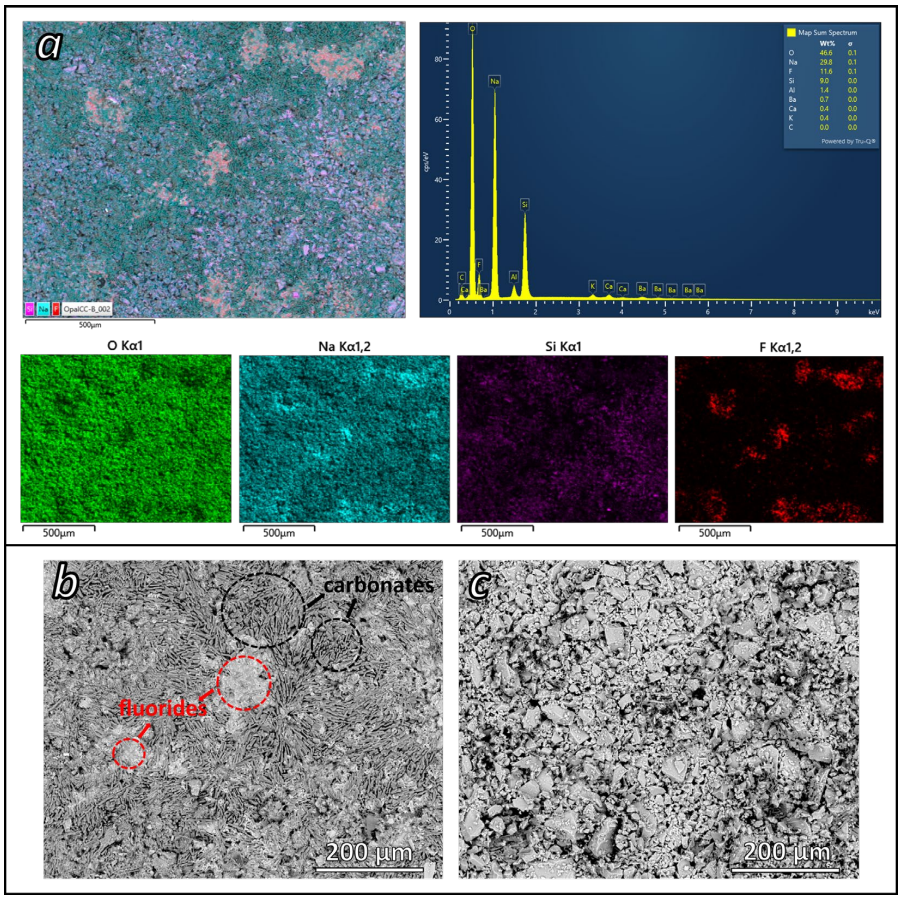

Figure 2. EDS analysis of consolidated opal glass product (**a**) and SEM images before (**b**) and after (**c**) boiling test.

Coarse fractions of discarded glass can be employed as passive components, acting not as reactive binders but as structural and decorative aggregates [30]. This approach is particularly relevant for the production of terrazzo-type composites, inspired by the historic Venetian terrazzo, which traditionally combines stone fragments and binders to create durable and ornamental flooring. In composite glass waste–based cements, the binder matrix may contain glass powders that partially substitute Portland cement, reducing

clinker content and associated CO_2 emissions [31,32]. Alongside these reactive fractions, coarser glass particles, sourced from post-consumer bottles, flat float glass, or other waste streams, can serve as inert inclusions. Their role is primarily physical: they provide bulk, texture, and color variation, enriching the composite's mechanical performance through aggregate interlock while also improving visual qualities [33].

In this study, coarse flakes of LCD glass and artistic SLG were added to the opal glass suspension after stirring. The consolidated samples show excellent mechanical compressive strength, reaching 29.6 ± 2.9 MPa for composites with artistic SLG. LCD and SLG filler particles are perfectly integrated within the opal glass matrix and form a compact (density: 1.94 ± 0.01 g/cm^3) and uniform structure with excellent aesthetic properties (Figure 3).

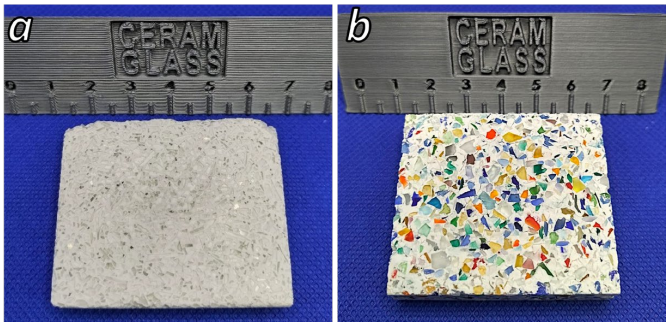

Figure 3. Opal glass-derived composites with inclusion of coarse LCD (**a**) and artistic SLG (**b**) particles.

A visual representation of the obtained results is shown in Figure 4. The chart illustrates the strength and density of commercial construction materials based on data from the latest release of Ansys CES (Cambridge Engineering Selector, EduPack, version 2025 R1). Newly developed opal glass-based cementitious composites are included as additional entries [26]. As expected, materials with higher porosity generally demonstrate lower strength values (corresponding to higher values of 1/compressive strength), and vice versa. Notably, the materials derived from opal glass (dense and composites) present particularly promising characteristics. They achieve compressive strengths comparable to cements and high-density concretes, but with lower densities. This combination of reduced density and enhanced mechanical resistance highlights the potential of opal-based binders as competitive alternatives within the construction materials landscape.

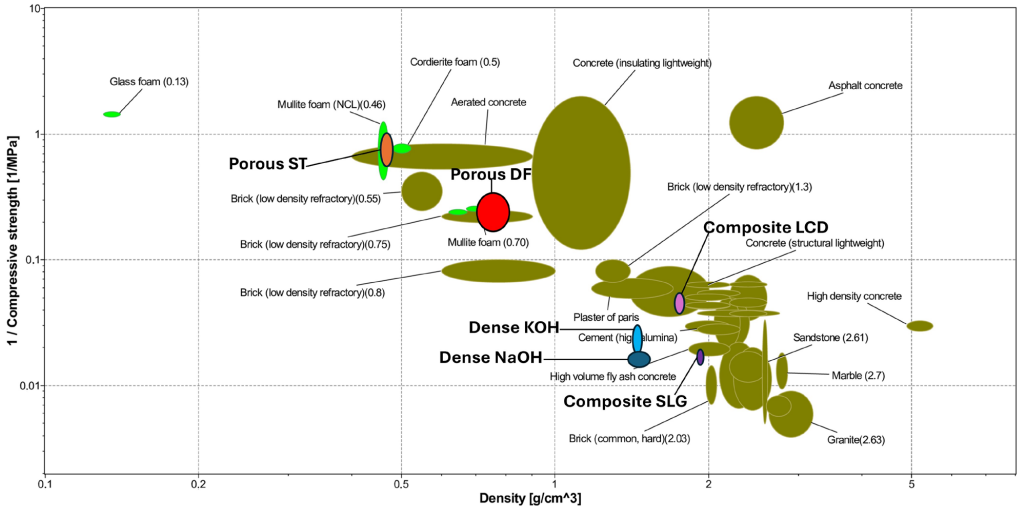

Figure 4. Compressive strength/density trade-off of activated opal glass products (computed by means of the CES software package, version 2025 R1).

3.2. Porous Products

Glass foams derived from alkali-activated waste glass constitute an emerging class of sustainable porous materials, offering a low-energy alternative to conventional high-temperature sintering routes [34]. In this approach, finely milled waste glass is subjected to alkaline activation, which induces partial dissolution of the amorphous silica network followed by polycondensation reactions that consolidate the structure at near-room temperature. The introduction of chemical foaming agents, such as hydrogen peroxide or metallic aluminum powders, promotes in situ gas evolution, while the addition of surfactants aids in stabilizing the nascent bubbles and regulating pore morphology [35]. This synergistic mechanism, usually accompanied by mechanical stirring, enables the formation of a lightweight, highly porous glass matrix with interconnected cellular structures and adequate mechanical cohesion, without requiring thermal treatment at high temperature. Consequently, alkali-activated glass foams exhibit promising functional characteristics—including low density, thermal insulation capacity, and potential acoustic attenuation—while simultaneously reducing energy demand and valorizing post-consumer glass waste within a circular economy framework [36].

3.2.1. Direct Foaming

Sodium perborate (SP) has been identified as an effective foaming agent for the synthesis of porous inorganic matrices, including alkali-activated waste glass and related geopolymeric systems, owing to its ability to undergo hydrolytic decomposition with concomitant oxygen release [37]. In aqueous alkaline environments, sodium perborate initially hydrolyzes, yielding hydrogen peroxide (H_2O_2) and borate species; the hydrogen peroxide subsequently decomposes into water and molecular oxygen under the catalytic effect of hydroxyl ions. This two-step decomposition pathway ensures a controlled and progressive release of O_2, which promotes pore nucleation and growth within the viscous activating medium [34,38]. The kinetics of gas evolution can be tuned by the concentration of sodium perborate, the alkalinity of the activating solution, and the curing conditions, thus controlling both pore size distribution and overall porosity. Sodium perborate offers several advantages, including reduced risk of uncontrolled exothermic reactions, absence of hydrogen evolution (thereby improving safety and environmental compatibility), and improved homogeneity of pore generation. The stabilization of oxygen bubbles is typically facilitated by surfactants like sodium dodecyl sulfate [39].

The addition of sodium perborate and sodium dodecyl sulfate (SDS) to the activated opal glass suspensions resulted in highly porous materials with homogeneous and interconnected pores (Figure 5). The inclusion of 1 wt% of SP and SDS led to a total porosity (mainly open) of 68.20% and a compressive strength of 2.6 ± 0.6 MPa (red circle in Figure 4).

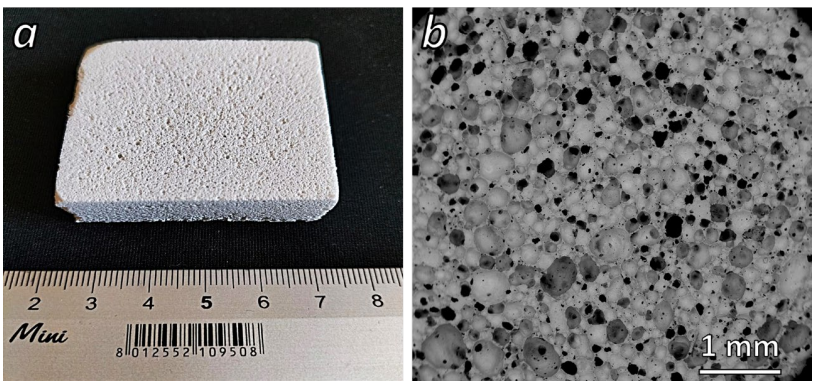

Figure 5. Macroscopic (**a**) and microscopic (**b**) images of a porous sample obtained from opal glass by direct foaming.

3.2.2. Salt-Templating Method

The salt-templating method has emerged as a versatile and effective approach for tailoring the porosity of alkali-activated materials (AAMs). According to this technique, soluble salts such as NaCl, KCl, or other inexpensive and non-toxic inorganic salts are incorporated into the precursor mixture during synthesis and subsequently removed, typically by water leaching, to generate a well-defined porous network [40]. Salt crystals act as a physical template, promoting the formation of interconnected pores depending on particle size and distribution. Compared to conventional foaming or surfactant-assisted methods, salt templating offers greater control over pore geometry, improved reproducibility, and scalability, while avoiding the introduction of additional organic agents that may compromise thermal stability [41]. Furthermore, the approach enhances mass transport properties and increases the specific surface area of alkali-activated matrices, making the resulting porous materials highly suitable for applications in adsorption, catalysis, and energy storage [37,42].

Salt templating resulted in highly porous specimens with open and interconnected pores (Figure 6). The salt crystals, along with the soluble carbonates (Na_2CO_3) that were generated during condensation reactions, are completely removed from samples after being kept in water at 60 °C. The difference in sample mass measured before and after water immersion was found to be consistent with the amount of salt initially added to the activated glass suspensions. This further confirmed the effectiveness of the salt removal process (~14, 16, 18, 20, and 24 g for the various formulations with 70, 80, 90, 100, and 120 wt% salt loading, respectively). Mineralogical analysis confirms that after three days of immersion, all peaks due to sodium chloride disappear without compromising the structure and composition of the final material (Figure 7).

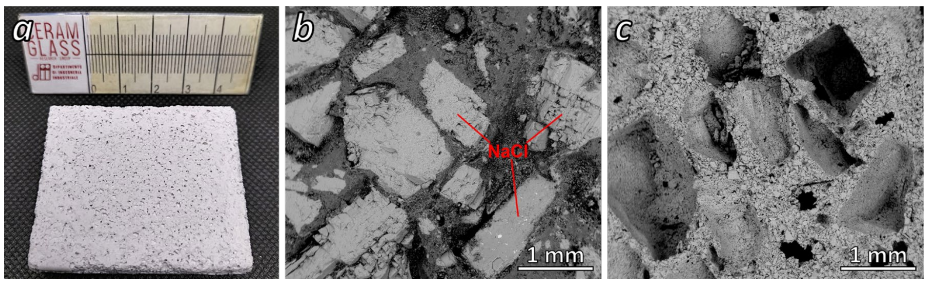

Figure 6. Opal glass porous sample produced by salt templating (**a**); SEM images of opal glass products before (**b**) and after (**c**) salt removal.

As shown in Figure 8, the total porosity of the samples increases linearly with the rise in the salt load added to the glass matrix after activation and then removed through water leaching. The significant increase in porosity, related to the large amount of salt added after the activation process, inevitably causes a reduction in the measured compressive strength of the final material. Samples containing 100 and 120 wt% of salt loading, initially activated with 2.5 M NaOH, were found to be extremely brittle, showing values of mechanical strength below 0.4 MPa. This behavior is attributed to the high amount of salt present in the system, which interferes with the activation reaction of glass particles and reduces the effectiveness of the alkaline activation process. As a result, the extent of matrix formation and particle bonding is significantly limited at lower activator concentrations. Increasing the molarity of the alkaline activator to 5 M in these last two formulations actually allowed us to overcome this limitation, significantly improving the mechanical properties of the porous specimens with a final compressive strength of 1.0 ± 0.2 MPa and total porosity of 80.09 ± 0.55% (corresponding to a density of 0.47 ± 0.01 g/cm^3). Physical and mechanical properties of the porous materials produced in this investigation are provided in Table 2.

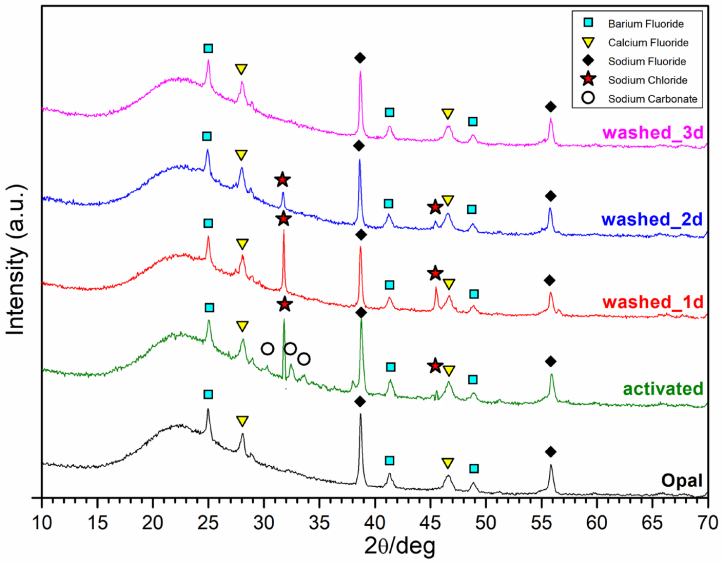

Figure 7. X-ray diffraction analysis of opal glass in the as-received state, after salt inclusion, and after 1, 2, and 3 days of immersion in hot water.

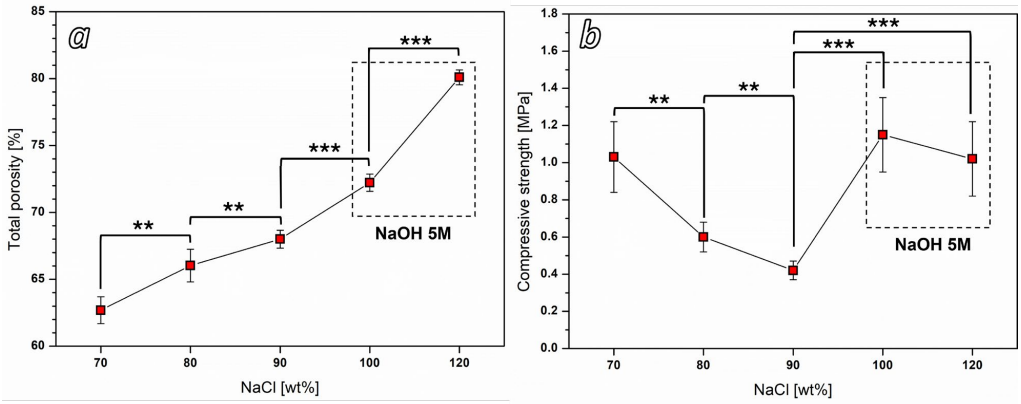

Figure 8. Total porosity (**a**) and compressive strength (**b**) as a function of increasing salt loading in opal glass-derived porous samples obtained by the salt-templating method. ** indicates a p-value < 0.01, *** p-value < 0.001 (MATLAB software, version R2025a).

Table 2. Physical and mechanical properties of opal glass porous products produced by direct foaming (DF) and salt templating (ST).

Sample		ϱ_{geom} [g/cm^3]	ϱ_{app} [g/cm^3]	ϱ_{true} [g/cm^3]	OP [%]	CP [%]	TP [%]	σ_{comp} [MPa]
Porous DF		0.76 ± 0.05	2.37 ± 0.01	2.39 ± 0.01	67.90 ± 1.98	0.30 ± 0.02	68.20 ± 1.95	2.6 ± 0.6
Porous ST	NaCl 70 wt%	0.95 ± 0.06	2.37 ± 0.01	2.39 ± 0.01	59.99 ± 2.58	0.23 ± 0.01	62.69 ± 2.57	1.0 ± 0.2
	NaCl 80 wt%	0.78 ± 0.02	2.36 ± 0.01	2.38 ± 0.01	65.81 ± 1.05	0.22 ± 0.01	66.03 ± 1.22	0.6 ± 0.1
	NaCl 90 wt%	0.70 ± 0.03	2.35 ± 0.01	2.37 ± 0.01	69.75 ± 1.89	0.25 ± 0.01	70.00 ± 0.37	0.4 ± 0.05
	NaCl 100 wt%	0.68 ± 0.01	2.42 ± 0.02	2.45 ± 0.02	72.88 ± 0.45	0.34 ± 0.01	73.22 ± 0.45	1.2 ± 0.2
	NaCl 120 wt%	0.47 ± 0.01	2.36 ± 0.01	2.39 ± 0.01	79.84 ± 0.55	0.25 ± 0.01	80.09 ± 0.55	1.0 ± 0.2

3.3. Chemical Stability

The chemical stability of dense and porous opal glass-based materials is confirmed by the results of leaching tests shown in Figure 9. According to legislated threshold values established by Italian Ministerial Decree 27 Sept 2010 and the EN 12457 standardized testing procedure [43], all opal glass-based products can be classified as non-hazardous and are eligible for disposal in a non-hazardous landfill. The choice of using the Italian regulation as a reference was made due to its stricter nature compared to those in other European countries. The measured concentrations are also consistent with those established at the European level by Council Decision 2003/33/EC for the acceptance of non-hazardous waste in landfills [44]. Specifically, for Ni, Cu, As, Mo, Sb, and Ba, the applied limit values are aligned with the European thresholds, as the Italian regulation directly implements the EU criteria. Regarding Rb and Sr, these elements are not explicitly regulated by European law; however, the measured concentrations are low and consistent with a non-hazardous classification. Between the two procedures followed for the production of porous materials, salt templating appears to consistently lead to the development of products that better withstand leaching tests, with noticeably lower releases of elemental components compared to samples developed via direct foaming.

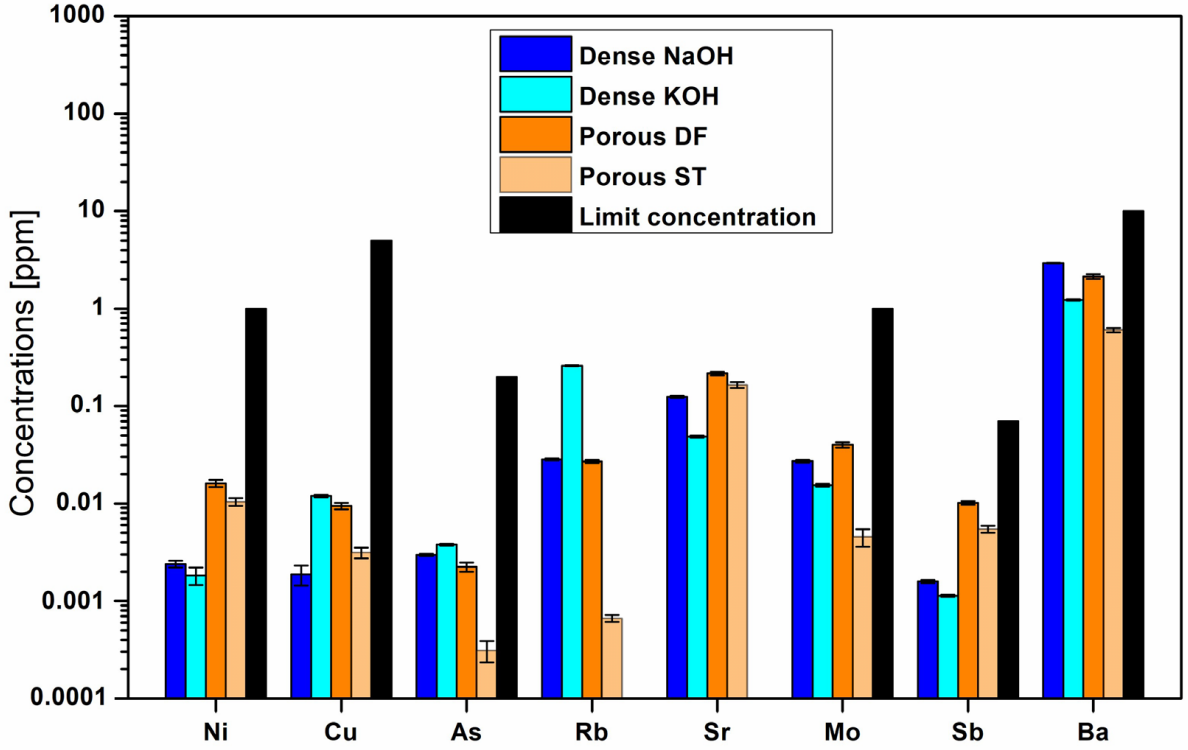

Figure 9. ICP-MS-derived concentrations of micro-components in leachates from alkali-activated materials based on opal glass waste. The black bars indicate the leachate concentration limits for disposal as non-hazardous waste according to Italian Ministerial Decree 27 September 2010.

3.4. Cytotoxicity and Antimicrobial Activity

The cytotoxicity test results for opal glass, dense KOH and NaOH samples, as well as porous ST, are reported in Figure 10a. Opal glass at a lower dosage (1 mg) shows CVI% below 20%, suggesting that it is not cytotoxic. This occurred even with dense KOH and NaOH (considering both the results with the lower amount of assayed sample), while at higher dosages (2 mg), opal glass showed a slight cytotoxicity effect, whereas dense KOH and NaOH at higher dosages showed moderate cytotoxicity. Since these samples are chemically stable (as confirmed by the leaching test), the reduction in cell viability is

related to the alkaline environment. Indeed, these samples showed pH values equal to 10 and 9.5 after 24 h of exposure. The alkaline effect is also confirmed by literature findings showing that a high alkaline pH (above 8) negatively affects HaCaT cell viability, as these cells normally grow in an acidic environment (physiological pH < 6) [45]. Indeed, it has been reported that HaCaT cells can tolerate exposure for 1 day in an alkaline environment up to pH 10.5, while no cells survive at pH above 11.5 [46]. Regarding porous ST, slight cytotoxicity was observed at both low and high dosages, which could be attributed to a slight increase in alkalinity (measured pH: 8).

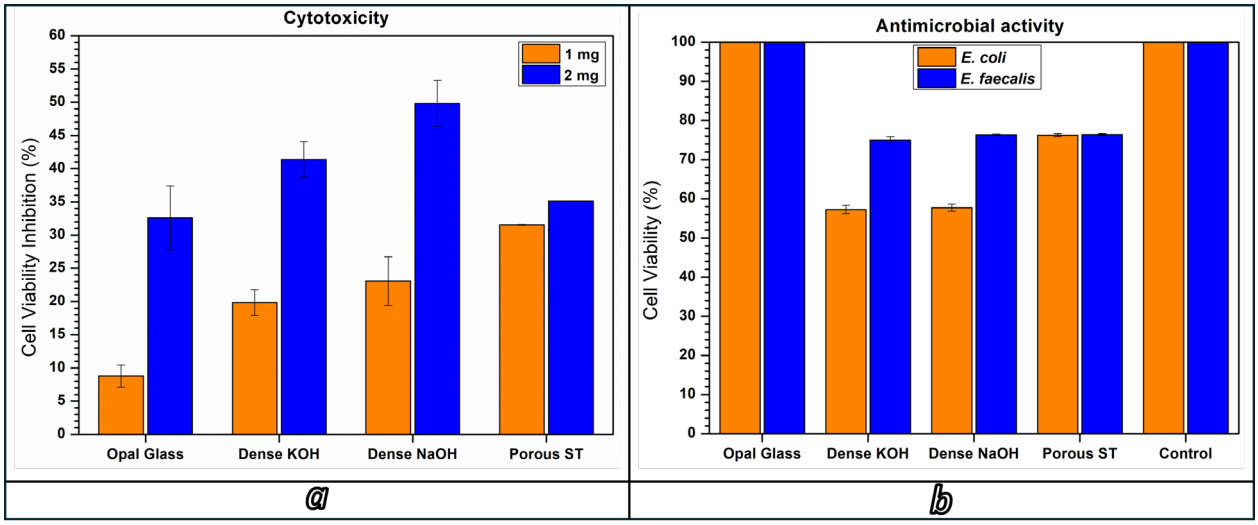

Figure 10. HaCaT cell viability inhibition (**a**) and microbial cell viability (**b**) of opal glass, dense KOH and NaOH, and porous ST samples after tests with both microbial and eukaryotic cells.

The non-cytotoxic effect of opal glass is also supported by the antimicrobial activity. Indeed, there was no inhibition halo for this sample when assayed in the presence of *E. coli* and *E. faecalis* (see Figure 10b). Moreover, the increase in antimicrobial activity (CV% below 60%) of dense KOH and NaOH with respect to *E. coli* is due to the alkaline environment (pH = 10 for both samples), which negatively affects the cell survival of this Gram-negative strain. In contrast, *E. faecalis*, which can react to alkali presence [47], showed only a reduction of 25% of cell viability. Finally, the low cytotoxicity of porous ST toward eukaryotes is also confirmed by its low toxicity toward prokaryotes since this sample showed a reduction of only 25% in cell viability against both the assayed Gram-negative and -positive strains.

3.5. Preliminary Assessment of Potential Application

The experimental results obtained in this study allow a first qualitative assessment of the potential practical applications of the developed opal glass-derived materials. Although a comprehensive application-oriented evaluation is beyond the scope of the present work, some preliminary considerations can be drawn. Dense alkali-activated opal glass products, particularly those activated with NaOH, exhibit a favorable combination of relatively low density (~1.47 g/cm^3) and high compressive strength (up to ~30 MPa). These characteristics suggest potential use as lightweight structural or semi-structural elements, as well as binder phases in glass-based cementitious systems. The good stability in boiling water further supports their possible application in humid or chemically aggressive environments.

Composite materials incorporating coarse LCD and soda-lime glass fractions showed improved densification and mechanical performance (~1.94 g/cm^3 and ~30 MPa), together with enhanced aesthetic features. These preliminary results indicate promising

applicability in decorative architectural elements, such as terrazzo-like surfaces, tiles, or prefabricated panels.

Porous materials developed via direct foaming and salt templating exhibit high total porosity (up to ~80%) and low density (down to ~0.47 g/cm^3), combined with sufficient mechanical integrity. These features make them suitable candidates for thermal and acoustic insulation, as well as lightweight fillers. The interconnected pore structure observed in both processing routes may also be advantageous for applications requiring permeability or mass transport, such as filtration or adsorption.

Finally, the positive outcomes of leaching and cytotoxicity tests suggest that the materials are environmentally compatible, supporting their potential use in construction and design applications involving human contact.

4. Conclusions

This investigation demonstrated that post-consumer unrecyclable opal glass can be successfully valorized through mild alkaline activation to obtain dense, composite, and porous materials with tailored properties under low-temperature processing conditions (60 °C curing and short microwave treatment).

Dense matrices activated with NaOH reached compressive strengths up to 30.3 ± 2.9 MPa at a density of 1.47 ± 0.06 g/cm^3, outperforming KOH-activated systems (22.2 ± 4.4 MPa) and confirming the more effective activation and gel formation promoted by sodium ions.

The incorporation of coarse LCD and soda-lime glass fragments generated composite systems with compressive strengths approaching 30 MPa and densities up to 1.94 ± 0.01 g/cm^3, while also providing attractive aesthetic features suitable for decorative and architectural applications.

Porous materials fabricated by direct foaming and salt templating achieved total porosities ranging from ~68% to more than 80%, with densities as low as 0.47 ± 0.01 g/cm^3 and compressive strengths between 0.4 and 2.6 MPa, maintaining sufficient mechanical integrity for lightweight applications.

The results confirmed that pore morphology and interconnectivity can be effectively tailored through the use of foaming agents, surfactants, and salt templates.

Leaching tests demonstrated that all investigated materials complied with Italian and European regulatory thresholds for non-hazardous waste classification. Preliminary cytotoxicity and antimicrobial assays indicated low toxicity and potential multifunctional behavior.

Overall, the study demonstrates the technical feasibility of upcycling opal glass waste into functional alkali-activated materials using relatively mild processing conditions and low-molarity alkaline activators.

As this work was conceived as an exploratory study, some limitations remain, particularly regarding the lack of long-term durability assessment, thermal conductivity measurements, permeability evaluation, detailed pore size distribution analysis, and advanced pore interconnectivity characterization. These aspects will be systematically investigated in future studies together with application-specific performance evaluations.

Author Contributions: Conceptualization, E.B., F.C., I.L., M.C., C.L., and L.B.; methodology, E.B., I.L. and M.C.; validation, E.B., I.L., M.C., F.C., E.D.R. and A.D.; formal analysis, F.C., E.D.R. and A.D.; investigation, E.B. and F.C.; resources, E.B., I.L. and M.C.; data curation, F.C., E.D.R. and A.D.; writing—original draft preparation, F.C.; writing—review and editing, E.B., I.L. and M.C.; visualization, F.C., E.B.; supervision, E.B., I.L. and M.C.; project administration, E.B., I.L. and M.C.; funding acquisition, E.B. All authors have read and agreed to the published version of the manuscript.

Funding: This investigation was specifically funded by the Italian Ministry of University & Research (MUR) in the framework of the GLASS_Trea.S.U.Res (GLASS-based TREAtments for Sustainable Upcycling of inorganic RESidues) project (PRIN 2022 PNRR project #P2022S4TK2).

Institutional Review Board Statement: Not applicable.

Informed Consent Statement: Not applicable.

Data Availability Statement: The original contributions presented in this study are included in the article. Further inquiries can be directed to the corresponding authors.

Conflicts of Interest: The authors declare no conflicts of interest.

References

1. Ramteke, D.D.; Hujova, M.; Kraxner, J.; Galusek, D.; Romero, A.R.; Falcone, R.; Bernardo, E. Up-cycling of 'unrecyclable' glasses in glass-based foams by weak alkali-activation, gel casting and low-temperature sintering. *J. Clean. Prod.* **2021**, *278*, 123985. [CrossRef]
2. Bristogianni, T.; Oikonomopoulou, F. Glass up-casting: A review on the current challenges in glass recycling and a novel approach for recycling "as-is" glass waste into volumetric glass components. *Glass Struct. Eng.* **2023**, *8*, 255–302. [CrossRef]
3. Luhar, S.; Cheng, T.W.; Nicolaides, D.; Luhar, I.; Panias, D.; Sakkas, K. Valorisation of glass waste for development of Geopolymer composites—Mechanical properties and rheological characteristics: A review. *Constr. Build. Mater.* **2019**, *220*, 547–564. [CrossRef]
4. Provis, J.L. Alkali-activated materials. *Cem. Concr. Res.* **2018**, *114*, 40–48. [CrossRef]
5. Chen, Y.; Zou, C.; Yong, C.L.; Jan, R.J.S.; Tan, T.H.; Lin, J.; Mo, K.H. Utilization of waste glass as precursor material in one-part alkali-activated aggregates. *J. Mater. Res. Technol.* **2024**, *33*, 5551–5558. [CrossRef]
6. Pascual, A.B.; Tognonvi, T.M.; Tagnit-Hamou, A. Optimization study of waste glass powder-based alkali activated materials incorporating metakaolin: Activation and curing conditions. *J. Clean. Prod.* **2021**, *308*, 127435. [CrossRef]
7. Ding, Y.; Dai, J.G.; Shi, C.J. Mechanical properties of alkali-activated concrete: A state-of-the-art review. *Constr. Build. Mater.* **2016**, *127*, 68–79. [CrossRef]
8. Gok, S.G.; Sengul, O. Mechanical properties of alkali-activated slag based SIFCON incorporating waste steel fibers and waste glass. *Constr. Build. Mater.* **2023**, *408*, 133697. [CrossRef]
9. Ricciotti, L.; Lucariello, D.; Perrotta, V.; Apicella, A.; Aversa, R. Sustainable Alkali-Activated and Geopolymer Materials: What Is the Future for Italy? *Recycling* **2025**, *10*, 140. [CrossRef]
10. Nikravan, M.; Firdous, R.; Stephan, D. Life cycle assessment of alkali-activated materials: A systematic literature review, Low-carbon Mater. *Low-Carbon Mater. Green Constr.* **2023**, *1*, 13. [CrossRef]
11. Hassan, A.M.; Bunnori, N.M.; Ramesh, S.; Tan, C.Y.; Mo, K.H. Glass-based foam from alkali activation: A review on effect of primary foaming parameters on microstructure and density. *Constr. Build. Mater.* **2024**, *427*, 136157. [CrossRef]
12. Baek, C.R.; Kim, H.D.; Jang, Y.C. Exploring glass recycling: Trends, technologies, and future trajectories. *Environ. Eng. Res.* **2025**, *30*, 240241. [CrossRef]
13. Tameni, G.; Bernardo, E. Alkali Activation of Glass for Sustainable Upcycling: An Overview. *Ceramics* **2025**, *8*, 108. [CrossRef]
14. Shi, X.; Liao, Q.; Liu, L.; Deng, F.; Chen, F.; Wang, F.; Zhu, H.; Zhang, L.; Liu, C. Utilizing multi-solid waste to prepare and characterize foam glass ceramics. *Ceram. Int.* **2023**, *49*, 35534–35543. [CrossRef]
15. Thomsen, L.; Jensen, L.R.; Yue, Y.; Østergaard, M.B. Crystallinity dependence of thermal and mechanical properties of glass-ceramic foams. *J. Eur. Ceram. Soc.* **2024**, *44*, 7936–7942. [CrossRef]
16. Aschoff, J.; Partschefeld, S.; Schneider, J.; Osburg, A. Effect of Microwaves on the Rapid Curing of Metakaolin- and Aluminum Orthophosphate-Based Geopolymers. *Materials* **2024**, *17*, 463. [CrossRef]
17. Rincón, A.; Marangoni, M.; Cetinb, S.; Bernardo, E. Recycling of inorganic waste in monolithic and cellular glass-based materials for structural and functional applications. *J. Chem. Technol. Biotechnol.* **2016**, *91*, 1946–1961. [CrossRef]
18. Ellison, A.; Cornejo, I.A. Glass Substrates for Liquid Crystal Displays. *Int. J. Appl. Glass Sci.* **2010**, *1*, 87–103. [CrossRef]
19. Lee, J.E.; Kim, E.; Hwang, J.B.; Choi, J.C.; Lee, J.K. Flake formation and composition in soda-lime-silica and borosilicate glasses. *Heliyon* **2023**, *9*, e16333. [CrossRef]
20. Bernardo, E.; Elsayed, H.; Mazzi, A.; Tameni, G.; Gazzo, S.; Contrafatto, L. Double-life sustainable construction materials from alkali activation of volcanic ash/discarded glass mixture. *Constr. Build. Mater.* **2022**, *359*, 129540. [CrossRef]
21. Contrafatto, L.; Gazzo, S.; Tameni, G.; Moro, L.; Bernardo, E. Engineered combinations of volcanic ash and waste glass for sustainable alkali activated materials. *J. Build. Eng.* **2025**, *112*, 113912. [CrossRef]
22. Rabelo Monich, P.; Rincon Romero, A.; Rambaldi, E.; Bernardo, E. Case studies of up-cycling of partially crystallized ceramic waste in highly porous glass-ceramics. *Constr. Build. Mater.* **2020**, *261*, 119971. [CrossRef]

23. *UNI EN 826:2013*; Thermal Insulating Products for Building Applications—Determination of Compression Behaviour. UNI: Milan, Italy, 2013.
24. *EN 12457-4:2002*; Characterisation of Waste—Leaching—Compliance Test for Leaching of Granular Waste Materials and Sludges—Part 4: One Stage Batch Test at a Liquid to Solid Ratio of 10 L/kg for Materials with Particle Size Below 10 mm (Without or with Size Reduction). European Committee for Standardization (CEN): Brussels, Belgium, 2002.
25. Piccolella, S.; Fiorentino, M.; Cimmino, G.; Esposito, A.; Pacifico, S. Cilentan *Cichorium intybus* L. organs: UHPLC-QqTOF-MS/MS analysis for new antioxidant scenario, exploitable locally and beyond. *Future Foods* **2024**, *9*, 100379. [CrossRef]
26. Fiorentino, M.; Piccolella, S.; Gravina, C.; Stinca, A.; Esposito, A.; Catauro, M.; Pacifico, S. Encapsulating *Calendula arvensis* (Vaill.) L. Florets: UHPLC-HRMS Insights into Bioactive Compounds Preservation and Oral Bioaccessibility. *Molecules* **2023**, *28*, 199. [CrossRef]
27. D'Angelo, A.; Viola, V.; Fiorentino, M.; Dal Poggetto, G.; Blanco, I. Use of natural dyes to color metakaolin-based geopolymer materials. *Ceram. Int.* **2025**, *51*, 5528–5535. [CrossRef]
28. Carollo, F.; Rienzo, E.D.; D'Angelo, A.; Sgarbossa, P.; Barbieri, L.; Leonelli, C.; Lancellotti, I.; Catauro, M.; Bernardo, E. Cold Consolidation of Waste Glass by Alkali Activation and Curing by Traditional and Microwave Heating. *Materials* **2025**, *18*, 2628. [CrossRef] [PubMed]
29. Tameni, G.; Lago, D.; Kaňková, H.; Buňová, L.; Kraxner, J.; Galusek, D.; Dawson, D.M.; Ashbrook, S.E.; Bernardo, E. Alkaline attack of boro-alumino-silicate glass: New insights of the molecular mechanism of cold consolidation and new applications. *Open Ceram.* **2025**, *21*, 100726. [CrossRef]
30. Liu, Y.; Shi, C.; Zhang, Z.; Li, N. An overview on the reuse of waste glasses in alkali-activated materials. *Resour. Conserv. Recycl.* **2019**, *144*, 297–309. [CrossRef]
31. Islam, G.M.S.; Rahman, M.H.; Kazi, N. Waste glass powder as partial replacement of cement for sustainable concrete practice. *Int. J. Sustain. Built Environ.* **2017**, *6*, 37–44. [CrossRef]
32. Ren, F.; Zhang, X.; Lin, M.; Wang, Q.; Sun, J. Recycling Local Waste Glass Bottles into Cement Paste: Effect on Hydration, Microstructure, and CO_2 Emission. *Materials* **2023**, *16*, 6195. [CrossRef]
33. Khan, K.; Ahmad, W.; Amin, M.N.; Rafiq, M.I.; Arab, A.M.A.; Alabdullah, I.A.; Alabduljabbar, H.; Mohamed, A. Evaluating the effectiveness of waste glass powder for the compressive strength improvement of cement mortar using experimental and machine learning methods. *Heliyon* **2023**, *9*, e16288. [CrossRef]
34. Hujova, M.; Monich, P.R.; Sedlacek, J.; Hnatko, M.; Kraxner, J.; Galusek, D.; Bernardo, E. Glass-Ceramic Foams from Alkali-Activated Vitrified Bottom Ash and Waste Glasses. *Appl. Sci.* **2020**, *10*, 5714. [CrossRef]
35. Kastiukas, G.; Zhou, X.; Wan, K.T.; Gomes, J.C. Lightweight Alkali-Activated Material from Mining and Glass Waste by Chemical and Physical Foaming. *J. Mater. Civ. Eng.* **2019**, *31*, 04018397. [CrossRef]
36. Ruan, S.; Kastiukas, G.; Liang, S.; Zhou, X. Waste Glass Reuse in Foamed Alkali-Activated Binders Production: Technical and Environmental Assessment. *Front. Mater.* **2020**, *7*, 581358. [CrossRef]
37. Wattanarach, S.; Supothina, S.; Thavorniti, P. Preparation and properties of metakaolin-based porous geopolymer formed with sodium perborate. *Asian Ceram. Soc.* **2022**, *10*, 567–574. [CrossRef]
38. Horvat, B.; Ducman, V. Potential of Green Ceramics Waste for Alkali Activated Foams. *Materials* **2019**, *12*, 3563. [CrossRef]
39. Korat, L.; Ducman, V. Characterization of Fly Ash Alkali Activated Foams Obtained Using Sodium Perborate Monohydrate as a Foaming Agent at Room and Elevated Temperatures. *Front. Mater.* **2020**, *7*, 572347. [CrossRef]
40. Shi, R.; Han, C.; Li, H.; Xu, L.; Zhang, T.; Li, J.; Lin, Z.; Wong, C.P.; Kang, F.; Li, B. NaCl-templated synthesis of hierarchical porous carbon with extremely large specific surface area and improved graphitization degree for high energy density lithium ion capacitors. *J. Mater. Chem. A* **2018**, *6*, 17057–17066. [CrossRef]
41. Klimek, A.; Réty, B.; Ghimbeu, C.M.; Frackowia, E. Impact of Disorder, Porosity, and Surface Chemistry of Salt Templated Carbons on Capacitance. *Adv. Sci.* **2025**, *12*, e05032. [CrossRef]
42. Longhi, M.A.; Zhang, Z.; Rodríguez, E.D.; Kirchheim, A.P.; Wang, H. Efflorescence of Alkali-Activated Cements (Geopolymers) and the Impacts on Material Structures: A Critical Analysis. *Front. Mater.* **2019**, *6*, 89. [CrossRef]
43. Council of the European Union. Establishing criteria and procedures for the acceptance of waste at landfills pursuant to Article 16 and Annex II to Directive 1993/31/EC. *Off. J. Eur. Commun.* **2003**, *11*, 27–49. Available online: https://eur-lex.europa.eu/legal-content/EN/TXT/PDF/?uri=CELEX:32003D0033&from=EN (accessed on 9 November 2025).
44. European Council. Council Decision 2003/33/EC of 19 December 2002 Establishing Criteria and Procedures for the Acceptance of Waste at Landfills Pursuant to Article 16 of and Annex II to Directive 1999/31/EC. *Off. J. Eur. Union* **2003**, *L11*, 27–49. Available online: https://www.legislation.gov.uk/eudn/2003/33 (accessed on 12 December 2025).
45. Lönnqvist, S.; Emanuelsson, P.; Kratz, G. Influence of acidic pH on keratinocyte function and re-epithelialisation of human in vitro wounds. *J. Plast. Surg. Hand Surg.* **2015**, *49*, 346–352. [CrossRef]

46. Galeotti, A.; Uomo, R.; Spagnuolo, G.; Paduano, S.; Cimino, R.; Valletta, R.; D'Antò, V. Effect of pH on in vitro biocompatibility of orthodontic miniscrew implants. *Prog. Orthod.* **2013**, *14*, 15. [CrossRef]
47. Padan, E.; Bibi, E.; Ito, M.; Krulwich, T.A. Alkaline pH homeostasis in bacteria: New insights. *Biochim. Biophys. Acta (BBA)-Biomembr.* **2005**, *1717*, 67–88. [CrossRef]